Eur. Phys. J. A (2025) 61:284
https://doi.org/10.1140/epja/s10050-025-01758-4

THE EUROPEAN PHYSICAL JOURNAL A

Regular Article - Experimental Physics

First operation of the FAMU experiment at the RIKEN-RAL high intensity muon beam facility

A. Adamczak[1], D. Bakalov[2], G. Baldazzi[3,4], M. Baruzzo[5], R. Benocci[6,7], R. Bertoni[6], M. Bonesini[6,8], S. Capra[9,10], D. Cirrincione[5], M. Clemenza[6,8], L. Colace[11,12], M. Danailov[5,13], P. Danev[2], A. de Bari[14,15], C. De Vecchi[15], D. Di Ferdinando[4], E. Fasci[16,17], R. Gaigher[6], L. Gianfrani[16,17], A. D. Hillier[18], K. Ishida[19], J. S. Lord[18], A. Menegolli[14,15,a], E. Mocchiutti[5], S. Monzani[5,20], L. Moretti[16,17], G. Morgante[3,21], C. Pizzolotto[5], A. Pullia[9,10], M. Pullia[15,22], R. Ramponi[9,23], H. E. Roman[6,8], M. Rossella[15], R. Rossini[14,15], A. Sbrizzi[3,4], M. Stoilov[2], J. J. Suárez-Vargas[5,25], G. Toci[24], L. Tortora[11], E. Vallazza[6], K. Yokoyama[18], A. Vacchi[5,19,20]

[1] Institute of Nuclear Physics, Polish Academy of Sciences, Radzikowskiego 152, 31342 Kraków, Poland
[2] Institute for Nuclear Research and Nuclear Energy, Bulgarian Academy of Sciences, blvd. Tsarigradsko ch. 72, 1784 Sofia, Bulgaria
[3] Dipartimento di Fisica e Astronomia "A. Righi", Università di Bologna, viale Berti Pichat 6/2, Bologna, Italy
[4] Sezione INFN di Bologna, viale Berti Pichat 6/2, Bologna, Italy
[5] Sezione INFN di Trieste, via A. Valerio 2, Trieste, Italy
[6] Sezione INFN di Milano Bicocca, Piazza della Scienza 3, Milano, Italy
[7] Dipartimento di Scienze dell'Ambiente e della Terra, Università di Milano Bicocca, Piazza della Scienza 1, Milano, Italy
[8] Dipartimento di Fisica "G. Occhialini", Università di Milano Bicocca, Piazza della Scienza 3, Milano, Italy
[9] Sezione INFN di Milano, via Celoria 16, Milano, Italy
[10] Dipartimento di Fisica, Università degli Studi di Milano, via Celoria 16, Milano, Italy
[11] Sezione INFN di Roma Tre, Via della Vasca Navale 84, Rome, Italy
[12] Dipartimento di Ingegneria, Università degli Studi Roma Tre, Via V. Volterra 62, Rome, Italy
[13] Sincrotrone Elettra Trieste, SS14, km 163.5, Basovizza, Italy
[14] Dipartimento di Fisica "A. Volta", Universitá di Pavia, via A. Bassi 6, Pavia, Italy
[15] Sezione INFN di Pavia, Via A. Bassi 6, Pavia, Italy
[16] Sezione INFN di Napoli, Via Vicinale Cupa Cintia 26, Napoli, Italy
[17] Dipartimento di Matematica e Fisica "L. Vanvitelli", Università della Campania, Viale Lincoln 5, Caserta, Italy
[18] ISIS Neutron and Muon Source, STFC Rutherford-Appleton Laboratory, Didcot OX11 0QX, UK
[19] Riken Nishina Center, RIKEN, 2-1 Hirosawa, Wako, Saitama 351-0198, Japan
[20] Dipartimento di Scienze Matematiche, Informatiche e Fisiche, Università di Udine, via delle Scienze 206, Udine, Italy
[21] INAF-OAS Bologna, via P. Gobetti 93/3, Bologna, Italy
[22] Centro Nazionale di Adroterapia Oncologica (CNAO), Via Borloni 1, Pavia, Italy
[23] IFN-CNR, Dipartimento di Fisica, Politecnico di Milano, piazza Leonardo da Vinci 32, Milano, Italy
[24] INO-CNR, via Madonna del Piano 10, 50019 Sesto Fiorentino, Italy
[25] Present Address: INFN LNS, Catania, Italy

Received: 15 September 2025 / Accepted: 22 November 2025

Communicated by Klaus Peters

Abstract The FAMU experiment, supported and funded by the Italian Institute of Nuclear Physics (INFN) and by the Science and Technology Facilities Council (STFC), aims to perform the first measurement of the ground-state hyperfine splitting (*1S-hfs*) of muonic hydrogen (μH). This quantity is highly sensitive to the proton's Zemach radius R_Z. An experimental determination of R_Z provides significant constraints on the parametrisation of the proton form factors as well as on theoretical models describing the proton's electromagnetic structure. Following years of technological and methodological development, the FAMU experiment began operations in 2023 at Port 1 of the RIKEN-RAL muon beam line at the ISIS Neutron and Muon Source facility (Didcot, UK). In this paper, we first describe the unique detection technique employed by FAMU to determine the *1S-hfs* of muonic hydrogen, followed by a detailed presentation of the final experimental layout. Finally, we report the first outcome from the 2023 commissioning run and from the initial physics runs performed in 2023 and 2024.

[a] e-mail: alessandro.menegolli@unipv.it (corresponding author)

Published online: 24 December 2025

1 Introduction

The results coming from the experiment on Lamb shift in muonic hydrogen μH which allowed derivation of the proton charge radius with unprecedented precision [1], contradicted measurements done with different techniques [2] based on extracting the proton charge radius from electronic hydrogen or elastic electron-proton scattering. This experimental result gave rise to the iconic *proton radius puzzle* and sparked a decade-long flurry of theoretical and experimental analyses, all of which agreed that additional research into the muonic hydrogen atom system was necessary. In fact, the energy levels of muonic hydrogen are orders of magnitude more sensitive to the details of the proton structure than the levels of normal hydrogen, since the reduced mass of the nucleus-muon system is 187 times bigger than that of the nucleus-electron system. This long-pursued laser spectroscopy measurement highlighted the sensitivity of the muonic hydrogen system, which can be regarded as an observatory capable of serving—depending on the transition considered and the precision achieved—as a cross-check for predictions in fields such as QED, nuclear physics, and particle physics. This result immediately revived the previous idea of using laser spectroscopy to measure the hyperfine splitting (*1S-hfs*) in the ground state of muonic hydrogen [3,4]. The hyperfine splitting in muonic hydrogen represents a case where the accuracy of QED calculations exceeds the accuracy of the known values of fundamental physical parameters. Hence the measurement of ΔE^{1S}_{hfs} provides a unique possibility for the measurement of the proton magnetic structure with high accuracy than that achievable in nuclear or particle physics experiments. The Zemach radius R_Z is the physical quantity related to the electromagnetic properties of the proton that can be extracted from the muonic hydrogen *1S-hfs* measurements. It can be expressed as:

$$R_Z = \frac{\Delta E^{1S-hfs}_{exp}/E^F - 1 - \delta^{QED} - \delta^{recoil} - \delta^{pol} - \delta^{hvp}}{2m_{\mu p}\alpha} \tag{1}$$

where $m_{\mu p}$ is the reduced mass of muonic hydrogen. E_F is the Fermi energy expressed in terms of muon and proton masses m_μ, m_p, and of the magnetic dipole moment of the proton μ_p:

$$E^F = \frac{8}{3}\alpha^4 c^2 \frac{m_\mu^2 m_p^2}{(m_\mu + m_p)^3}\mu_p \tag{2}$$

while δ^{QED}, δ^{recoil}, δ^{pol} and δ^{hvp} are correction terms related to the proton electromagnetic structure and to the strong interaction [5]. The Zemach radius of the proton R_Z is defined in terms of the first moment of the convolution of the charge $\rho_E(\mathbf{r})$ and magnetic moment distributions $\rho_M(\mathbf{r})$ [6]:

$$R_Z = \int d^3\mathbf{r}|\mathbf{r}| \int d^3\mathbf{r}' \rho_E(\mathbf{r}')\rho_M(\mathbf{r}-\mathbf{r}') \tag{3}$$

The hyperfine splitting of μH is the quantity that is most sensitive to the proton's Zemach radius R_Z. The experimental value of R_Z places significant constraints on the parametrisation of proton form factors as well as the theoretical models of proton electromagnetic structure [5,7]; the measurement of the *1S-hfs* in the μH system is therefore essential [8,9]. A method was originally drawn up at a time when the laser system could not be produced with the necessary performance [3]. A possible approach [10] was subsequently identified by the FAMU (Fisica Atomi MUonici—Physics of Muonic Atoms) collaboration, supported and funded by the Italian Institute of Nuclear Physics (INFN) [11,12].

The paper is organised as follows: in Sect. 2 the technique proposed by the FAMU experiment to measure the *1S-hfs* in the μH system is presented, highlighting previous achievements of the FAMU Collaboration towards the definition of the final setup of the experiment, which is illustrated in all its components in Sect. 3. The first operation of the FAMU experiment, which took place in 2023 at the Port 1 of the RIKEN-RAL muon beam at the ISIS Neutron and Muon Source facility (Didcot, UK), is presented in Sect. 4, with a particular emphasis put into the commissioning phase of July 2023 (Sect. 4.1) and on the first runs for physics of 2023 and 2024 (Sect. 4.2). Conclusions and perspectives are finally summarised in Sect. 5.

2 The FAMU experiment

Different experimental proposals for the measurement of ΔE_{1S-hfs} in the $1S$ state of the μH system have been put forth in recent years to provide top-accuracy data on the Zemach radius of the proton [13–15]. This has been motivated by the need for new data on the proton electromagnetic structure that, as we have seen, had become a problem with the proton charge radius determination from the Lamb shift in muonic hydrogen. The laser excitation of the ortho $F = 1$ hyperfine sub-level of the ground state of the muonic hydrogen atom from the para $F = 0$ sub-level is the challenging task. This is a very weak $M1$ magnetic dipole transition with probability P of only

$$P = 2 \cdot 10^{-5}(E[J])(S[m^2])^{-1}(T[K])^{-1/2} \tag{4}$$

with E laser pulse energy, S laser beam cross section and T target temperature [11]. In order to increase the likelihood of this laser-induced transition to a detectable level, an

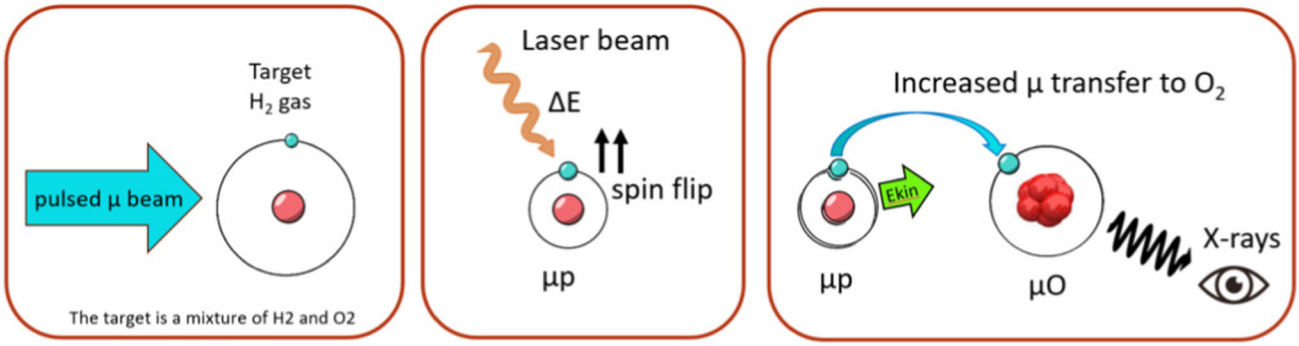

Fig. 1 Scheme of the FAMU method to excite the *1S-hfs* transition in muonic hydrogen through a MIR laser beam, with the subsequent transfer of the muon to molecular Oxygen and the detection of the typical μO X-rays as a signature of the transition

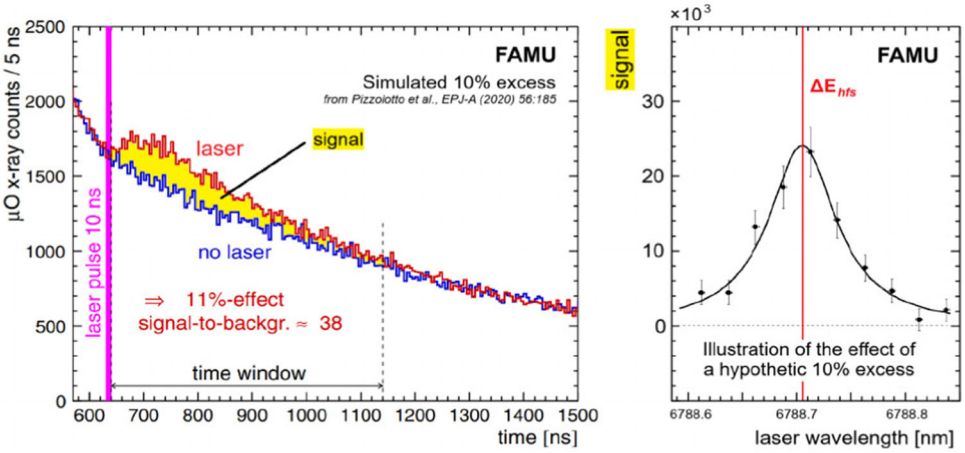

Fig. 2 Behaviour of the FAMU observable, the excess of delayed μO X-rays. Left: toy simulation of a hypothetical $\sim$10% effect on the FAMU observable (yellow coloured area). Right: illustration of a hypothetical resonance of the FAMU observable as a function of the laser wavelength, where the mean value is the resulting estimation of ΔE_{1S-hfs} (the value chosen here as ΔE_{1S-hfs} is the latest theoretical prediction, not a FAMU experimental result)

optical multi-pass cavity must be used. The muonic hydrogen atom is excited from the ground singlet to the triplet state with a laser, tunable around the resonance frequency $\Delta E_{1S-hfs}/h \sim 44$ THz. The experimental method, adopted by the FAMU Collaboration, uses a peculiar characteristic of the muon transfer between muonic hydrogen and oxygen molecules, to detect when the muonic hydrogen atoms are excited by the laser. For this reason, at first muonic hydrogen atoms are formed in a mixture of oxygen and hydrogen and then interact with a laser radiation tuned to a frequency around the hyperfine transition resonance, see Fig. 1. Finally, collisions of μH with oxygen lead to the reaction:

$$\mu H + O \rightarrow \mu O^* + H \tag{5}$$

The observable quantity used as signature of this reaction is the time distribution of the muon transfer events from hydrogen to oxygen [15], which are identified through the characteristic X-rays emitted during the de-excitation of the muonic oxygen. The maximum deviation of this X-ray time distribution from the time distribution in absence of the laser indicates that the laser source is tuned at the resonance frequency, see Fig. 2. The μH atoms that have been excited to the triplet state with the laser pulse are accelerated, after the de-excitation in subsequent collisions with the surrounding H_2 molecules, by nearly 0.12 eV; the atoms carry the released energy away as kinetic energy. Since the rate of muon transfer to oxygen $\lambda_{pO}(E)$ varies with the μH kinetic energy E [16], the observed time distribution of the characteristic X-rays is perturbed as compared to the time distribution in the absence of laser radiation; the resonance frequency is recognised by the maximal response of the X-ray time distribution. The efficiency of this method of detecting the events of laser-induced hyperfine excitation of the μH depends on how much the rate of muon transfer from accelerated μH atoms exceeds the transfer rate from thermalised atoms. The hydrogen-oxygen mixture had been selected for the FAMU method because of the evidence for a sharp energy dependence of $\lambda_{pO}(E)$ at thermal and near epithermal energies (nearly an order of magnitude) [16], that is not observed in other gases.

High precision spectroscopy is required to accurately identify this extremely weak transition signal and, in order to recover the signal, all potential background sources must be reduced to a minimum. This called for thorough simulations before building the final layout. The pulsed muon beam will penetrate the cryogenic target full of high purity hydrogen with low oxygen contamination, primarily forming

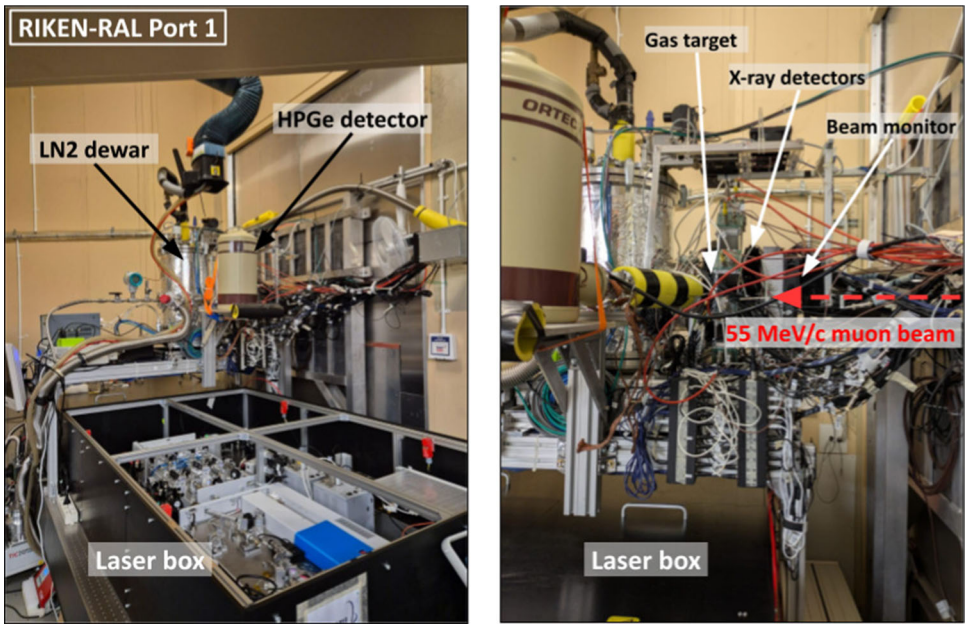

Fig. 3 Left: photograph of the fully mounted FAMU experiment at RIKEN-RAL Port 1, taken in September 2023 after the commissioning but before the first beam time. Right: zoom on the FAMU target and detectors

muonic hydrogen that quickly de-energises and reaches the atomic ground level, as happens to all other muonic atoms generated by the stray muons. A mosaic of specialised detectors, covering the majority of the solid angle seen by the target, progressively records the flow of the X-rays. The injection into the target of the laser radiation starts the actual measurement once the μH atoms have reached a thermal equilibrium with the surrounding gas. The multi-pass optical cavity that encloses the majority of the target's gas volume increases the transition probability, as it will be discussed later. When the appropriate wavelength inducing the transition is attained, the time distribution of the muonic oxygen X-rays will abruptly change, given the energy dependence of the muon transfer rate from hydrogen to oxygen $\lambda_{pO}(E)$ [11]. The typical time of this chain of processes to occur is of the order of few hundreds of nanoseconds.

The proposal of the FAMU experiment was presented in 2013 at the Program Advisory Committee (PAC) of the RIKEN laboratory, co-owner at that time of the RIKEN-RAL pulsed muon beam facility. After the approval of this first declination of the FAMU program, two subsequent competing proposals with the same physics target have been proposed and approved by other muon facilities [17,18]. Since 2013, the FAMU Collaboration devoted several fruitful data taking at the RIKEN-RAL facility, showing that the proposed method, the beam characteristics, and the selected detection systems were all suited to perform the μH *1S-hfs* measurement, as described in a series of papers illustrating both technical and scientific results [19–23]. In particular, the FAMU Collaboration was able to: confirm the suitability of the transfer method for the oxygen [24]; investigate different gas configurations to determine the best final setting (i.e. the type and quantity of high Z element in gas mixture and the values of pressure and temperature of the gas target); estimate the minimal duration of a run in the final configuration.

3 The FAMU experimental setup

The essential elements of the FAMU setup are as follows: a high rate, tunable momentum, pulsed muon beam monitored by a custom beam monitor; a Hydrogen-Oxygen mixture gas target kept at cryogenic temperature; a mid-infrared laser system; an optical cavity to maximise the number of laser excitations inside the gas target; a system of X-ray detectors made by scintillating crystals read either by Photo-Multiplier Tubes (PMTs) or by Silicon Photo-Multipliers (SiPMs) arrays; a custom DAQ system allowing the event collection and storage. A photograph of the FAMU full setup installed in the Port 1 of the RIKEN-RAL muon facility, taken after the June 2023 beam commissioning, is shown in Fig. 3.

3.1 Muon beam characteristics and monitoring

The ISIS Neutron and Muon Source is currently the leading centre in Europe for the production of pulsed neutron and muon beams. The facility is located at the Harwell Campus in Didcot, Oxfordshire (UK), as part of the Rutherford Appleton Laboratory (RAL). The ISIS muon beam [25,26] is produced by the collision of an 800 MeV proton beam with a target. The protons, accelerated inside the ISIS proton synchrotron, are extracted and directed to two different neutron production areas: Target Station 1 (TS1) and Target Station 2 (TS2). The proton beam extraction is carried out with a rate

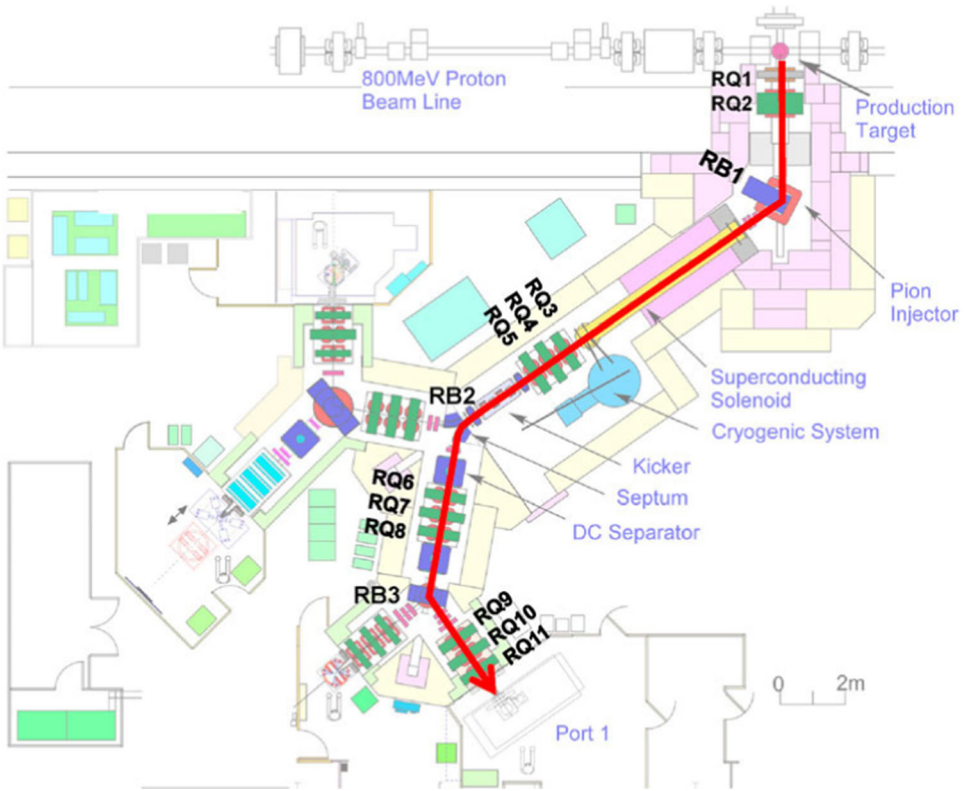

Fig. 4 Scheme of the path followed by muons directed to the FAMU target in the RIKEN-RAL muon facility. The positions of the bending (RB) and quadrupole (RQ) magnets involved in the beam delivery to FAMU are labelled

of 50 Hz, extracting particles from two proton bunches. For this reason, a proton spill is extracted every 20 ms, and it is composed of two proton bunches separated by 320 ns. Every five proton spills, four are sent to TS1 and one to TS2. As a consequence, the average repetition rate of protons against the muon production target is 40 Hz. The pions produced in the muon production target by protons hitting a graphite target will decay with a time constant of ~ 26 ns into muons and neutrinos, giving rise to the desired muon beam. Depending on whether the pions decay at rest inside the target or escape it, two species of muons can be extracted:

- surface muons are μ^+ originated from the decay at rest of π^+ produced close to the surface of the graphite target. The intensity is generally high (over 10^6 muons/s), their momentum peaks at about 29 MeV/c, as they are produced at rest.
- decay muons are μ^+ or μ^- formed by transporting the pions out of the target, selecting their desired momentum, and letting them decay in order to produce a muon beam of a certain momentum. They are sent to the RIKEN-RAL muon facility, with a momentum-dependent beam intensity (see Fig. 4). RIKEN-RAL is capable of delivering muons between 17 and 120 MeV/c. In particular, the beam delivered to FAMU is a 55 MeV/c decay μ^- beam.

The FAMU observable, consisting of the time distribution of the muon transfer events from hydrogen to oxygen as described in Sect. 2, is strongly dependent on the intensity of the muon beam injected into the target, which changes the number of muonic hydrogen atoms formed. As a consequence, the presence of a beam monitor in FAMU is clearly crucial both for beam control and data normalisation. For this purpose, after a series of prototypes described in references [27–29], a scintillating fibre-based hodoscope has been implemented as the muon beam monitor for the FAMU experiment. It was designed and built by INFN Milano Bicocca, INFN Pavia and INFN Roma3. It consists of two planes of polystyrene scintillating fibres (with perpendicular directions) read out on one side by a Hamamatsu S12751-50P SiPM, with 50 μm cells, see Fig. 5. The detector's fiducial area is $64 \times 64\,\text{mm}^2$. The 1 mm-pitch fibres are model BCF-12 by Bicron/Saint-Gobain/Luxium, with blue scintillation light (peak wavelength 435 nm), 3.2 ns of decay time, and a light yield of $\sim$ 8000 photons/MeV for Minimum Ionising Particles (MIPs). The fibres, with white TiO_2 EMA (Extra Mural Absorber) coating, 10–15 μm thick, to avoid cross-talk and interspaced by 1 mm from each other, are read-out on alternate ends by SiPMs soldered on four Printed Board Circuits (PCBs). Each PCB provides the same bias to all 16 SiPMs and fans out the 16 signals through MCX connectors. In the FAMU Data Acquisition System, hodoscope signals

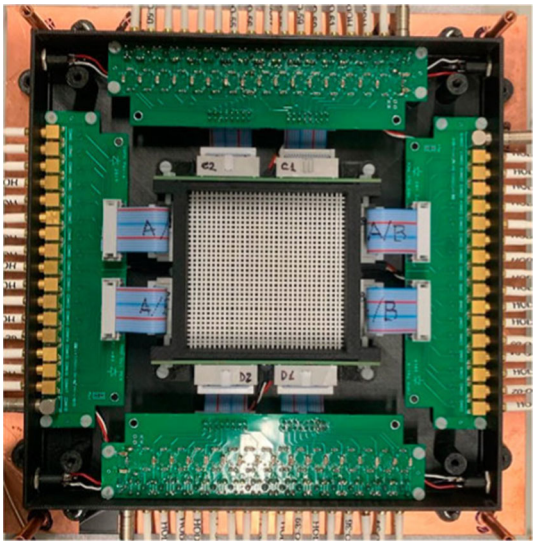

Fig. 5 Internal view of the FAMU beam monitor: the 32+32, 1 mm width scintillating fibres with TiO_2 EMA paint coating can be seen in the middle

are fanned out through MCX connectors and acquired using two CAEN V1742 digitisers (32 channels, 5 GS/s, 12 bit).

This detector, initially designed for beam focusing and centering, is now capable of measuring the muon beam intensity. This has been made possible by measuring the total charge deposited in the detector fibres during a beam spill (Q_{tot}) and taking into account the detector geometry and the muon energy loss at fixed 55 MeV/c momentum. For this specific geometry, the intensity can be calculated as $\varphi[s^{-1}] = k\,Q_{tot}$[ADC ch.], where the constant k is calculated as:

$$k = \frac{r\ [\mathrm{Hz}]}{(W_2 + \frac{W_1}{\eta})\ Q_\mu\ [\text{ADC ch.}]}. \tag{6}$$

Here, r is the fixed average beam repetition rate (40 Hz), Q_μ is the average charge deposited by a single muon interacting with two fibres, determined experimentally through a dedicated measurement [30], and $(W_2 + W_1/\eta)$ is a simulated correction factor taking into account the fraction W_j of muons interacting with $j = 1,2$ fibres, and the ratio η between the charge released in two fibres over that in one fibre.

The muon intensity measurement enables on-line beam line monitoring and data normalisation as a function of the number of muons entering the gaseous target. Fig. 6 shows a linearity plot for the beam monitor, in which the value of Q_{tot} is compared to the number of X-rays measured by the FAMU detector system, which is proportional to the number of muons on target, hence on the intensity. The right plot shows a set of intensity estimations as a function of momentum in the FAMU magnet setting.

3.2 Target system and multi-pass optical cavity

The kinetic transfer of the muon to oxygen acts as a background contribution to FAMU, as previously observed by FAMU in dedicated test beams at RAL. The experiment would ideally work at the lowest possible temperature for the hydrogen-oxygen mixture. However, the condensation temperature for O_2 limits the temperature to be above ~ 60 K. For this reason, it has been decided to use liquid nitrogen (77 K) as the target cooling medium. The target is filled with hydrogen with a percentage of oxygen of 1.5% which, combined with a pressure of 7 bar, is the optimal choice for the 80 K target temperature [12].

The target cryostat was designed to best satisfy all the FAMU requirements, namely: a thin high-Z muon beam entrance window, in order to maximise the momentum loss in the entrance window and therefore the muon capture in the gas; low-Z materials in other directions to let 100–200 keV X-rays out of the target, where detectors are placed; an optical window, needed to inject the laser beam, and fitting an optical cavity to maximise the gas-laser interaction. The current target has been simulated, optimised, designed and mounted in collaboration with CRIOTEC Impianti Srl to match the requirements. A lateral section of the FAMU target cryostat is shown in Fig. 7. In particular, the chamber containing the gas is shown in green and it is cooled by thermal contact with a tank containing 5 l of liquid nitrogen at 77 K. This solution enables vibration-free cooling, which is crucial to avoid laser misalignments during the experimental runs. In order to monitor the gas condition, the target chamber is equipped with a pressure sensor (sensitivity 0.01 mbar) and two temperature sensors (sensitivity 1 mK). These sensors play an important role in assessing the tightness of the chamber and correcting for small gas leakage.

The muon beam exits the beam pipe, crosses the FAMU beam monitor and then passes through a beam collimator composed of lead bricks. It is aimed at injecting the muon beam only in the central area of the target within the Multi-pass Optical Cavity (MOC). Muons enter the cryostat through a 0.2 mm aluminated Mylar window, then cross the 1 mm-thick aluminium wall of the gaseous target chamber, and lastly encounter a 0.6 mm layer of silver. The role of this Ag layer is to maximise the number of muons stopping in the gas by slowing them down just before entering the volume illuminated by the laser. Each mirror of the MOC [12] is constituted by three parts of Fused Silica coated with ZnS/Ge multi-layers to provide the best possible reflectivity $R = 99.890(2)\%$ at 6.78 μm. The three parts of the mirrors are designed in order to confine the light inside the cavity with a quasi-chaotic pattern. For this purpose the ends of the mirrors have a cylindrical shape while the central part has a flat surface. The MOC is aimed to enhance the transition probability by a factor of $1/(1-R)$, compared to Eq. 4. It is

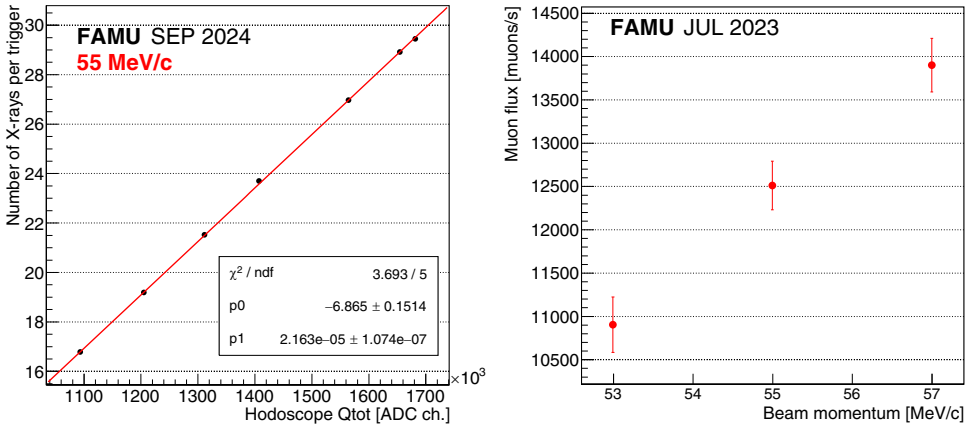

Fig. 6 Left: beam monitor intensity linearity, tested by varying the beam intensity through a dedicate de-tuning of bending magnet RB1, and comparing the charge deposited in the scintillating fibres (Q_{tot}) to the number of X-rays per trigger measured by the detectors, which is proportional to the number of muonic atoms in the target, hence to the muon intensity. Error bars are plotted but they are smaller than the data points. Right: measurement of the momentum-dependent muon beam intensity around the FAMU working point, measured in the standard FAMU focusing condition

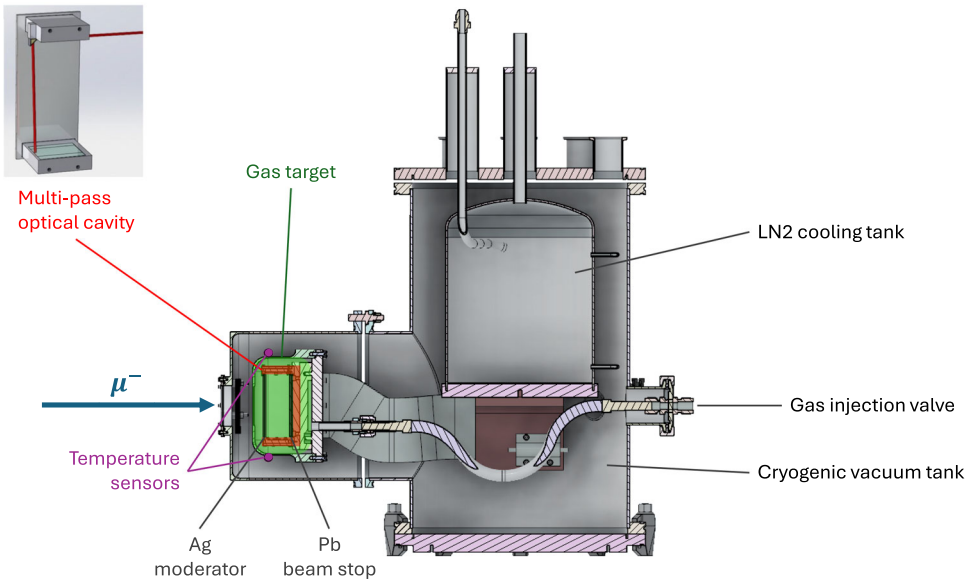

Fig. 7 Side section view of the target cryostat (CAD drawing), where the main components are marked. The three detector-holding rings are attached to the target cryostat around the target chamber (green volume), as shown in Fig. 10

studied to let the laser beam bounce back and forth, minimising its power loss. The alignment of the laser beam within the MOC is a very complex operation related to the fact that the MOC is closed inside the target that in operating condition is at T = 80 K and P = 7 bar. Therefore an alignment procedure has been realised by using a "twin" MOC placed outside the target as a reference. The laser beam, from the optical table, is sent into the target by means of a lift (periscope) composed by two Off-Axis Parabolic Mirrors (OAPM). One of the OAPM is mounted on the table while the second one is in "L" shape aluminium mount directly connected to the target chamber. A beam splitter plate can be housed for alignment purposes between the OAPM#2 and the window of the target chamber.

Figure 8 shows a sketch of the target ensemble with the external cavity on the side. The reference cavity is mounted on a roto-translation stage at the same height as the target cavity, and it is placed on an aluminium support on the right side of the periscope. The target cavity is aligned by superimposing the reflected beam merging from the target cavity with the reflected beam exiting from the reference cavity with a visible laser beam at 632 nm. The alignment procedure is carried out in two steps. First, we move the reference cavity with respect to a laser beam that hits orthogonally on the bottom mirror of the target cavity, in order to overlap the beams reflected from the two cavities. This ensures that both cavities are aligned to the same position relative to the laser beam.

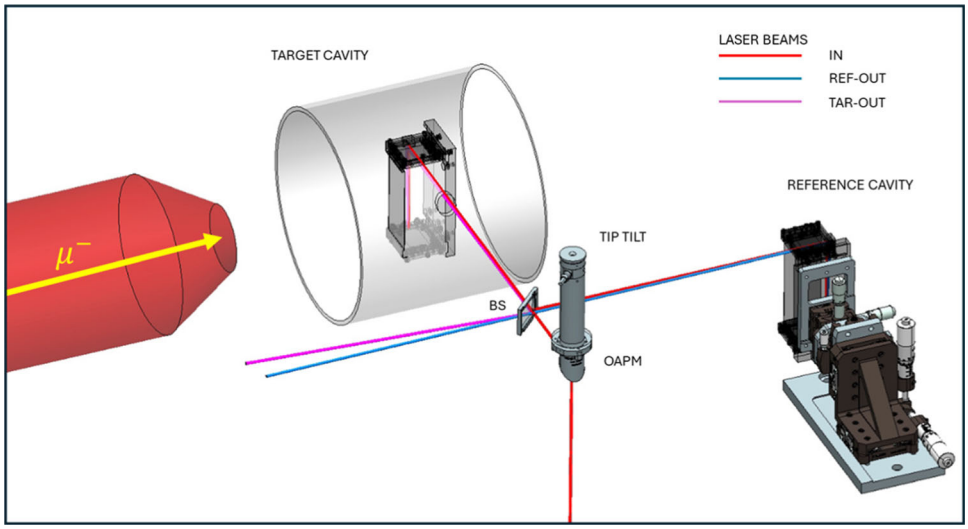

Fig. 8 Laser Injection Systems: sketch of the alignment procedure: a red laser beam, well overlapped with the 6.8 μm radiation, is directed towards the two identical Multi-pass Optical Cavity, namely the *reference cavity* and the *target cavity*. The injection is assured by aligning the reference cavity in a multi-pass optical configuration, being sure that the laser arrives at both cavities exactly the same way. BS stands for Beam Splitter and OAPM stands for Off-Axis Parabolic Mirror

Then, we align the target cavity in a multi-pass configuration by monitoring the optical path in the reference cavity:

- a visible laser (red) is injected in the target cavity and, by adjusting the position OAPMs, a configuration with a back reflection overlapped on the input one is obtained. In this way the laser beam impinges orthogonally on the bottom mirror of target cavity.
- A beam splitter at 45° is introduced after the OAPM #2. The laser beam is split in two parts and sent to two cavities. The distance between the beam splitter and the two injection mirrors is the same.
- By means of translators, rotators, and monitoring the spots of reflected light emerging from the two cavities, the reference cavity is aligned in the same way of target cavity. This step guarantees that the optical path in the reference cavity is the same as that in target cavity.
- By moving the OAPMs with motorised tip/tilt, the number of reflections in the reference cavity is maximised, guaranteeing that the optical path in the target cavity will be very similar.
- The visible beam laser is switched off, the beam splitter is removed and the infrared laser is injected in the target cavity.

3.3 Narrowband mid-infrared pulsed laser

The FAMU laser system, extensively described in [31], is a custom-made Mid Infra-Red (MIR) laser system, whose main characteristics are: wavelength around 6789 ± 3 nm, energy over 1 mJ, linewidth below 0.07 nm, tunability step below 0.03 nm, pulse duration below 10 ns and 25 Hz repetition rate. The FAMU laser performs excellently and exceeds the goal requirements in terms of energy, linewidth, and tunability step. The rate is half of the synchrotron rate in order to inject the laser every other beam spill, and use the spills with no laser as a background measurement. As of 2024 and to the best of our knowledge, the FAMU laser system is the most powerful pulsed 6.8 μm source available, combining narrow linewidth and fine tunability, and capable of delivering over 1.5 mJ of energy. The setup consists of two lasers: a fixed 1064 nm Nd:YAG Master-Oscillator-Power-Amplifier (MOPA), and a tunable (1262 ± 5) nm Cr:forsterite oscillator, which is then further injected in a 16-passes 3-stages Cr:forsterite amplifier. The Cr:forsterite oscillator includes a diffraction grating, and the two cavity mirrors are placed on piezoelectric motors in order to allow the adjustment of the wavelength. The two beams are then properly coupled and injected in a non-linear Difference Frequency Generator (DFG), in this case a crystal of barium-gallium selenide ($BaGa_4Se_7$). The output of the crystal is a laser beam with frequency given by the relation $\lambda_{DFG}^{-1} = \lambda_{Nd:YAG}^{-1} - \lambda_{Cr:forst}^{-1}$, which is in the required wavelength range. By tuning the wavelength of the Cr:forsterite laser it is therefore possible to tune the MIR wavelength for the experiment. The entire system can be monitored remotely via dedicated software, specifically designed to interface with a set of sensors. Based on their feedback, the system can be adjusted either automatically or manually using piezo motors. A schematic layout of the FAMU laser system is shown in Fig. 9. The laser was designed and perfected by INFN Trieste in collaboration with Elettra Sincrotrone in Trieste (Italy) and then installed, characterised extensively and further improved at RAL in collaboration with Università della Campania/INFN Napoli [32–35].

3.4 X-ray detectors

The X-ray detection system of the FAMU experiment requires:

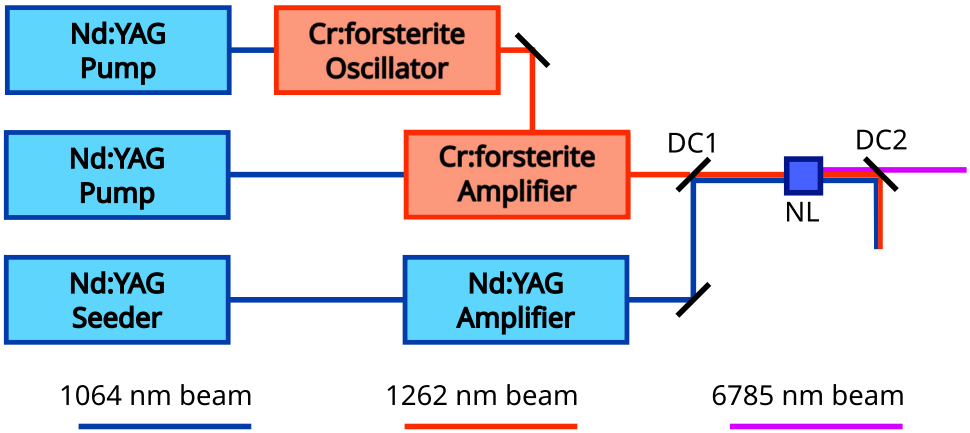

Fig. 9 Simplified sketch of the FAMU laser system representing the pump and signal formation and the coupling of the beams inside the non-linear (NL) crystal. DC1 and DC2 are dichroic mirrors used respectively to superimpose the beams and to isolate the 6.78 μm

– a good energy resolution at low energy (∼130–150 keV) to detect the signal muonic oxygen lines;
– a short signal fall time (less than 200–300 ns) to separate the delayed muonic X-rays (signal) from the prompt background and to reduce the signal pile-up;
– a large solid angle coverage to increase statistics.

The FAMU experiment makes use of different types of crystal detectors, arranged in three rings around the target chamber along the beam line and pointing to the centre of the optical cavity. All these detectors are based on lanthanum bromide doped with cerium scintillating crystals ($LaBr_3$:Ce) and have different read-out systems. Detectors with PMT readout were developed at INFN Bologna, while the ones with SiPM array readout were conceived and built at INFN Milano Bicocca, in collaboration with INFN Pavia. The FAMU setup for the 2023 data taking (so called *setup A*) is based on 34 such detectors positioned around the target as shown in Fig. 10:

– six 1″ diameter, 1″ thick cylindrical crystals read by Hamamatsu R11260-200 PMTs with a custom high voltage divider ("*LaBr*") [36];
– sixteen 1″ diameter, 1/2″ thick cylindrical crystals read by Hamamatsu S14161-6050-04-AS SiPM arrays ("*MIB045-MIB063*") [37,38];
– twelve 1/2″ cubic detectors read by Hamamatsu S13361-3050-04-AS SiPM arrays ("*MIB071-MIB099*") [39,40].

The six detectors with PMT readout are placed in the central ring, together with six 1″ detectors with SiPM array readout. The remaining ten 1″ detectors with SiPM array readout are placed in the upstream ring, while the cubic 1/2″ ones are positioned in the downstream ring [41].

In the 2024 data taking, the twelve 1/2″ cubic $LaBr_3$:Ce *MIB* detectors were replaced by 1″ diameter, 1/2″ thick cylindrical detectors with SiPM array readout, increasing the solid angle coverage by ∼ 30 % in one of the regions with the highest statistics of delayed oxygen X-rays (so called *setup B*) [42]. The detectors with SiPM array readout have a better FWHM energy resolution, as compared to the ones with PMT readout (see Table 1), at the cost of a slower fall time. This last feature has prompted a long R&D to reduce the detectors' fall time. While the 1/2″ detectors with a SiPM readout made use of conventional parallel ganging, the 1″ detectors use an innovative 1–4 circuit from Nuclear Instruments srl, that reduces the fall time by a factor of two, as shown in [37,43]. In this layout, the 1″ SiPM array is divided into four sub-arrays, by using four nearby $6 \times 6\,mm^2$ SiPM cells . Output signals from these are summed together and then amplified with pole-zero compensation. In this way, the capacitances are reduced. At the end, the four sub-array signals are summed together and inverted to produce a positive output. To handle the temperature increase (∼ 5–7 °C) due to the used TI 695 op-Amplifier (∼ 1W) a heat power dissipater had to be put in thermal contact with the backside of the used PCBs and an ad-hoc ventilation system had to be introduced in Port 1.

As explained in reference [44], the SiPM gain drifts as a function of a varying temperature. To keep it stable, a custom system, based on CAEN A7585 power supplies with temperature feedback, was studied, as reported in reference [45]. As the temperature in Port 1 is kept stable within ∼ ±1 °C and the temperature coefficient of Hamamatsu SiPM arrays is quite small (−34 mV/C), up to now, this online correction system has not been used. Possible residual gain drift of detectors with a SiPM read-out, during extended data taking periods, has been corrected offline by calibrations with the beam data themselves. At the end of this procedure, initial variations at the few percent level have been reduced to zero. Further details on the performance in the beam for these detectors are reported in reference [46].

A commercial ORTEC GEM-S5020P4 High Purity Germanium (HPGe) detector was also installed to accurately identify the peaks observed in the spectrum, thanks to its excellent energy resolution. This, in turn, allows for a better

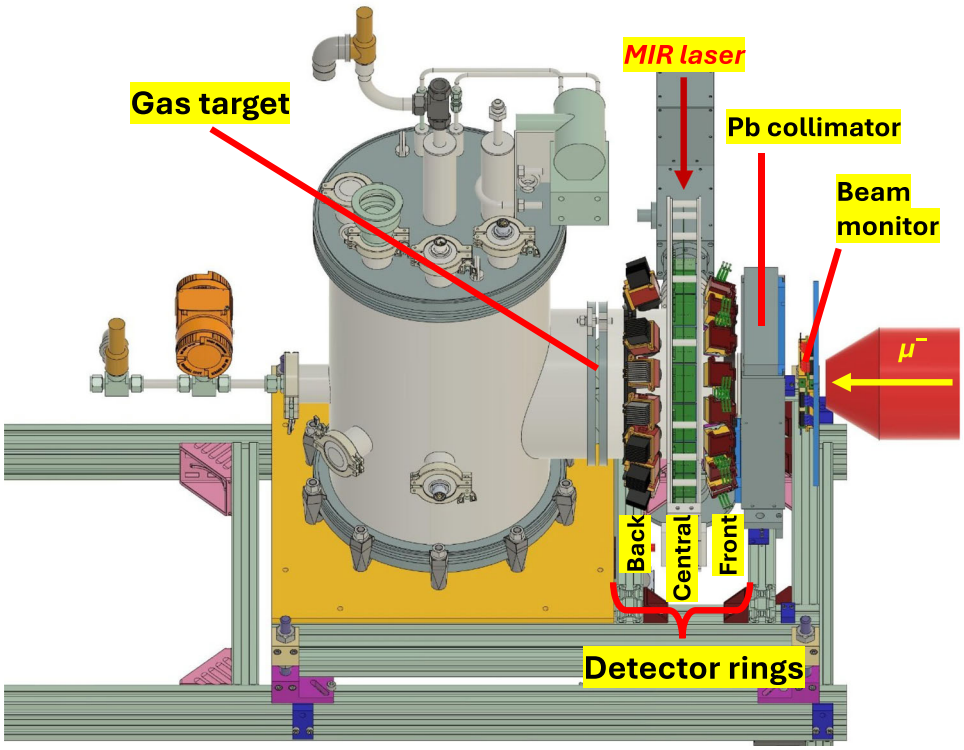

Fig. 10 Position of the three detector rings in the FAMU setup. The HPGe detector is omitted for improved illustration clarity

Table 1 Performances of the full set of installed detectors in terms of rise and fall times

	Rise time (ns)	Fall time (ns)	FWHM(%) @ 662 keV	FWHM(%) @ 122 keV	FWHM(%) @ 141 keV
1″—PMT	14 ± 1	~ 60	3.5–4.6	7.2–8.1	12.3 ± 1.2
1″—SiPM	29.3 ± 1.5	147.1 ± 12.8	2.94 ± 0.14	8.03 ± 0.39	7.0 ± 0.3
1/2″—SiPM	42.8 ± 4.7	372.4 ± 17.4	3.27 ± 0.11	8.44 ± 0.63	7.5 ± 0.3

Moreover, FWHM energy resolutions are indicated for the gamma ray lines of 662 keV (^{137}Cs), 122 keV (^{57}Co) and 141 keV (muonic silver). Sample averages and RMS deviations are reported

interpretation of the signals from the LaBr detectors, which have a poorer resolution. The timing and FWHM energy resolution of the three types of detectors are shown in Table 1. FWHM energy resolutions, for detectors with SiPM readout, at 662 keV ^{137}Cs and 122 keV ^{57}Co lines are from laboratory measurements at INFN Milano Bicocca, while at 141 keV (one of the muonic silver lines) are from beam data at RAL with 55 MeV/c impinging muons. For comparison, the FWHM energy resolution at the 141 keV muonic silver line is $(1.26 \pm 0.17)\%$ from the HPGe detector, at the cost of a much longer fall time. 10–90% rise time and fall time are measured at the 662 keV ^{137}Cs line.

3.5 Trigger and data acquisition

The data acquisition system of FAMU (FAMU-DAQ) [47] handles six digitisers in two VME crates outside Port 1, to digitise all the required signals. Fig. 11 shows a scheme of the readout system for each type of detector in the FAMU setup, together with a picture of the main VME crate. The whole DAQ system is triggered by the muon beam and specifically by the Cherenkov scintillators placed in a straight-on position beyond the bending magnet in the pion injection system, detecting gammas and higher energy charged particles from the muon production target. The beam hodoscope signals are fanned out from the detector with 64 MCX connectors and each of them is digitised. Two CAEN V1742 digitisers (32 channels, 5 GS/s, 12 bit) are used for this purpose, limited at 1 GS/s. All the signals coming from the scintillators, regardless of their readout system (PMT, SiPM Array + 4-1 circuit), are fanned out through MCX connectors and digitised using a total of six CAEN V1730/V1730S ADCs (8 channels,v500 MS/s, 14 bit). The HPGe detector long signals are acquired with a CAEN V1724 (8 channels, 100 MS/s, 14 bit) in order to digitise over a longer time window and lower sampling rate. In particular, the signal is digitised both as-it-is and with a shaping carried out with an ORTEC 672 amplifier with 3 μs shaping time.

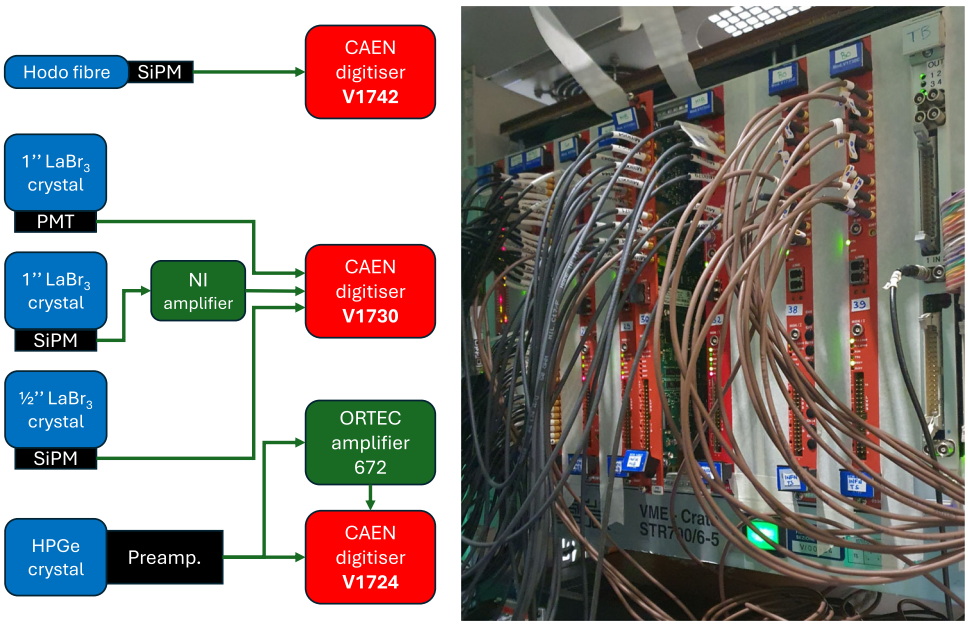

Fig. 11 Scheme of the DAQ electronics for all types of detectors (beam monitor fibres, scintillating crystals with different readout and HPGe detector) and close-up view of the main VME crate hosting the digitisers

The trigger system allows three modes of operation: random trigger for hardware debug, external NIM trigger for normal beam operation and external TTL trigger for calibration. In particular, the latter is used to calibrate detectors with radioactive sources: one channel is used as a source of the TTL trigger signal, which is then distributed to all digitisers through a trigger board. During normal beam operation, instead, a NIM signal coming from the Cherenkov detectors in the pion beam line is distributed to the digitisers by the same trigger board. The FAMU data acquisition system saves data in raw ROOT files, also called raw files. The software writes a file every 400 events, and 500 files (i.e. 200k events) form a run. At this stage, data processing is carried out on-line through a custom program which runs on all raw files, producing the so-called second-level files which are used for the high-level analysis.

The Cherenkov trigger used for the X-ray detector is not suitable for the laser, that needs a longer time to respond to generate light for illuminating the muonic hydrogen. The three laser sources that produce the 6.78 μm light each require two triggers, one to excite the active medium and the other to activate the Pockels Cell (PC), which initiates the laser pulse. The first trigger, commonly known as the Lamp trigger, must be sent to the laser system 140–150 μs before the laser pulse, while only 500 ns elapses between the PC trigger and the laser shot. The Cherenkov trigger arrives 500 ns after the muon's arrival, when the muonic hydrogen has already formed, making it incompatible with the laser system's trigger-to-shot timing.

Instead, the laser system uses a signal directly from the ISIS extractor, the device responsible for sending protons to the target stations. This signal reaches Port 1 approximately 3.5 μs before the muons arrive, providing enough time to serve as the trigger source for the PC. The previous extractor trigger is used for the lamp trigger. A scheme of the laser trigger is shown in Fig. 12. Another characteristic of the laser is that it operates at 25 Hz, rather than 50 Hz like ISIS, requiring it to fire once every two muon pulses. The laser data required by the experiment, energy and wavelength measured shot-to-shot, are collected with a different computer with respect to the X-rays. The laser events are triggered by the trigger board through a microcontroller that is connected to the computer via a serial connection. The microcontroller also collects the event number from the trigger board, enabling a one-to-one match of the laser and X-ray DAQ events.

4 First operations at Port 1

The first beam time assigned to the FAMU experiment by the scientific committees of the ISIS Neutron and Muon Source in July 2023 was used as a run for the beam, target, laser and commissioning of the full setup. Therefore, no physics data acquisition was made. After the FAMU successful commissioning phase at Port 1, the run for physics started with two beam times in October and December 2023, followed by two further beam times in 2024, for a total of 49 days of operations. Each data taking period was divided in batches, where a batch is defined as the set of contiguous measurements taken with the same laser wavelength: a batch number "*Batch N*" is then used to uniquely identify each data sample within the same data taking period.

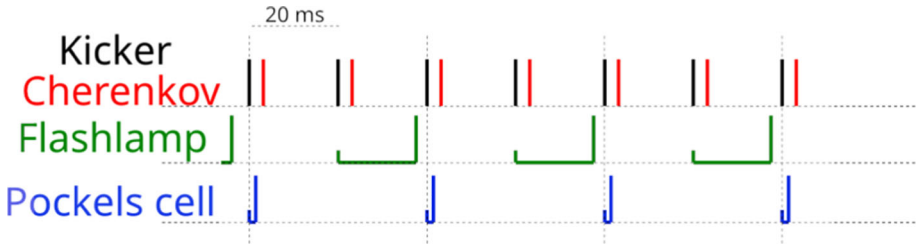

Fig. 12 The diagram illustrates the working principle of the laser trigger. Since the Cherenkov trigger arrives after the muons, it cannot be used to activate the laser. Instead, the solution is to use the kicker trigger: the PC is triggered by a signal that arrives 3.5 μs before the muons, while the flashlamps are activated by the previous kicker signal

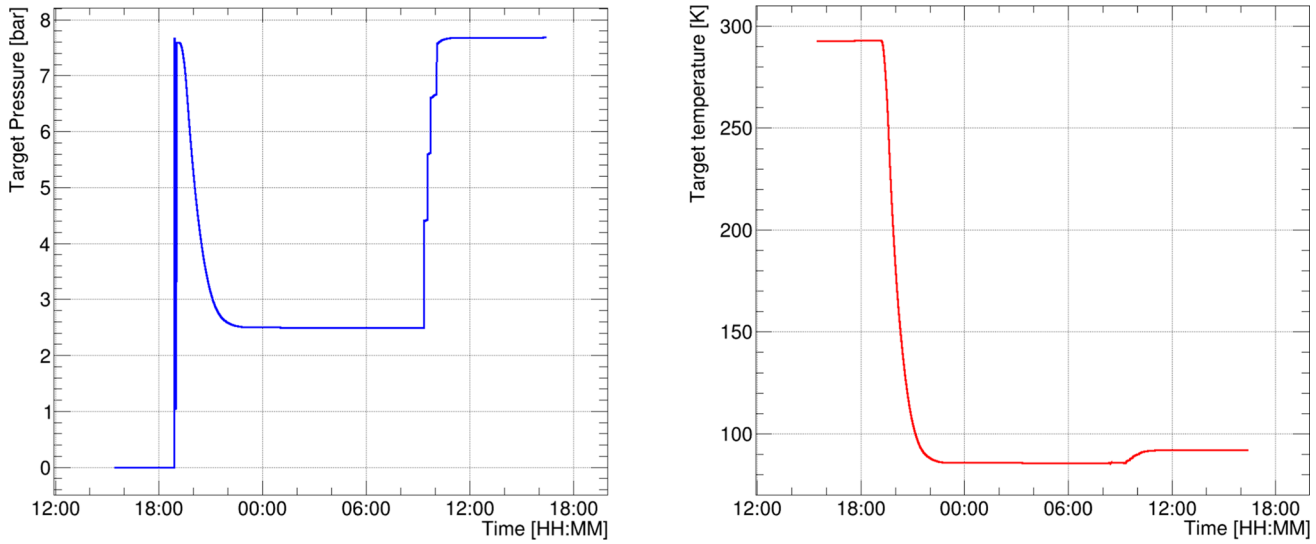

Fig. 13 Measured target pressure (left) and target temperature (right) as function of time during target filling and cooling

4.1 FAMU commissioning run

The FAMU setup installation began already in 2019, but forced stops and delays were caused first by the COVID-19 pandemic and then by the ISIS facility long-shutdown for the TS1 project, completed in 2022. FAMU installation was completed by mid 2023, and the commissioning run was held from July 17th to July 23rd, 2023. The first operation consisted of the gas target emptying, filling and cooling with the H_2/O_2 mixture.

The procedure is illustrated in Fig. 13. The left panel shows the pressure measured in the target as a function of time. Before data collection, the target is evacuated to remove any residual gas. Then, it is cleansed by filling it twice with the gas mixture, followed by evacuation each time (the corresponding lines cannot be distinguished in the figure). Finally, the target is filled with the gas mixture to approximately 7.5 bar, and the cooling process begins by filling the apparatus tank with liquid nitrogen. The right panel of Fig. 13 displays the target temperature. As seen in the figure, the temperature drops from room temperature (approximately 290 K) to about 85 K within a couple of hours. Consequently, the pressure in the target decreases to around 2.5 bar. The system stabilises within a few hours. In this example, we allowed it to stabilise overnight, though a couple of hours would have been sufficient. After the stabilisation period, the target is slowly refilled to 7.5 bar using a stepwise procedure (as shown in the left panel of Fig. 13) to verify the optical cavity alignment. As the gas quantity in the target increases, thermal dispersion through the optical window also rises, causing the target temperature to increase from 88 K to approximately 91 K. This temperature provides a sufficient gap relative to the de-excitation kinetic energy to observe the expected signal. The target system remains stable throughout the entire data taking period, with temperature fluctuations of less than one degree and a slow pressure decrease of less than 2% over two weeks.

Before each FAMU beam time, all X-ray detectors are calibrated online with radioactive sources of ^{241}Am (60 keV gamma ray), ^{133}Ba (multi-γ with main peaks at 31 keV, 81 keV, 356 keV) and ^{137}Cs (662 keV gamma ray). To do so, the muon beam is off and the trigger is given by the detector

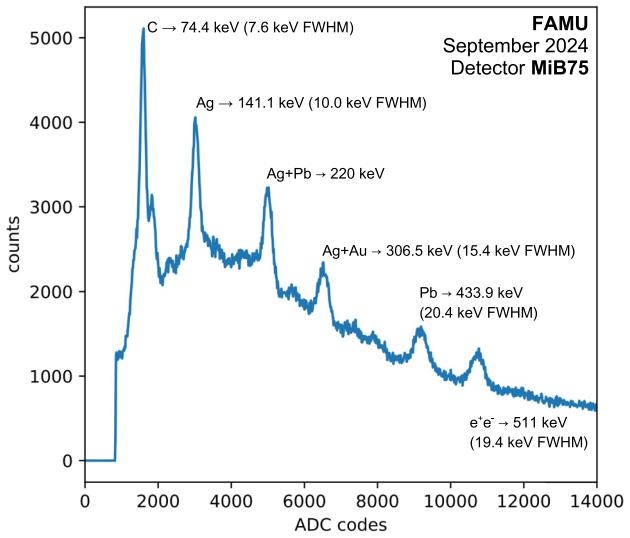

Fig. 14 Example of prompt X-rays from muon atoms of the material composing the FAMU target. The 511 keV prompt peak of e^+e^- annihilation is also highlighted

signals themselves. The calibration sources are positioned wherever space is available, according to the mechanical and geometrical constraints of the setup. A more refined offline semi-automatic calibration procedure allows then to reconstruct the spectral lines and to evaluate the time-dependence of the gain of each detector throughout the entire data taking period of the FAMU experiment. The gain variation is monitored by looking at the lines of the prompt muonic captures on the materials composing the target. Fig. 14 shows an example of an energy spectrum in ADC counts for one of the 1" *MIB* detectors.

As can be seen in Fig. 15, the gain of almost all detectors is stable at the few percent level. Fig. 16 indicates that *LaBr* detectors have a larger energy resolution (about 12%) compared to *MIB* detectors (about 7%), despite their better gain stability over time. Part of the worse FWHM energy resolution of the PMT-read LaBr3:Ce detectors is probably due to PMT currents being above the nominal values during operation at large X-ray fluxes. Fig. 17 shows the calibrated energy spectra obtained by summing the pulses from all detectors of the same type (*LaBr* and *MIB*). Thanks to the offline calibration procedure, the energy resolution measured in the sample, obtained by combining all detectors of the same type, is consistent with the average energy resolution of the single detectors.

The optimal muon beam momentum was finally selected in order to maximise the number of muons stopping inside the gas. This FAMU beam commissioning was accomplished by a fine tuning of the magnets of the RIKEN-RAL beam line, followed by the observation of prompt X-rays, coming from the de-excitation of muonic Oxygen atoms, calibrated with the radioactive sources as described above, see Fig. 18.

4.2 FAMU runs for physics

The first two beam times for physics took place in October and December 2023 for a total of 17 days. The spectral region covered by these data acquisitions is shown in Fig. 19 (left) and compared to the latest theoretical predictions for the *1S-hfs* wavelength [48–51]. In particular, 14 wavelengths have been measured in 2023 with the required statistics (at least 21–22 h of live time) and spanning from 6788.550 nm to 6788.875 nm. The fourth and fifth beam times followed in July and October 2024, respectively, allowing for the further extension of the range of the scanned wavelengths up to 29, from 6788.400 to 6789.050 nm. The total statistics of the triggers collected by FAMU in these four periods is reported in Table 2.

The off-line data analysis is a key part of the experiment as it allows selecting the information contained in the collected events to extract detector performance and the data required to construct the plot of the signal as a function of the laser wavelength as already shown in Fig. 2. Methods developed to get the final resonance plot using the first runs for physics are here briefly described and first preliminary results are shown.

The histogram of the laser wavelengths measured during 2023 is shown in Fig. 19 (right). The histogram is made with the instantaneous value of the wavelength saved for each event. The wavelength is varied in steps of 25 pm, as this optimal step allows for scanning the largest portion of the wavelengths without missing the signal, which is expected to be $\sim$ 80 pm wide [14]. It is important to notice that narrower and more regular peaks are visible for December 2023. This is thanks to an automatic wavelength keeper which was added to the laser software to optimise the laser stability [52]. Fig. 20 (left) demonstrates the wavelength stability: each point of the plot represents the average of the wavelength over one hour of data taking.

Figure 20 (right) shows a typical distribution of the energy delivered by each laser pulse. It is essential to recognise that the transition probability is proportional to the laser energy, as it is proportional to the number of photons interacting with the μH atoms. For this reason, the energy distribution must be considered when selecting data and comparing events with different energies. The system is not capable of delivering the same energy for every wavelength and this variation among different batches has to be considered for data normalisation.

An example of the performance of the X-ray detectors is shown in Fig. 21, where the number of X-rays collected in the Oxygen signal region (60–200 keV) by the $LaBr_3$:Ce read by SiPM arrays is shown as a function of the wavelength. The number of X-rays quoted in the plot is normalised on the number of muon triggers. The initial statistics (December 2023), about 0.8 X-rays per trigger and per wavelength point, have been then increased up to $\sim$ 1 in the latest run (September

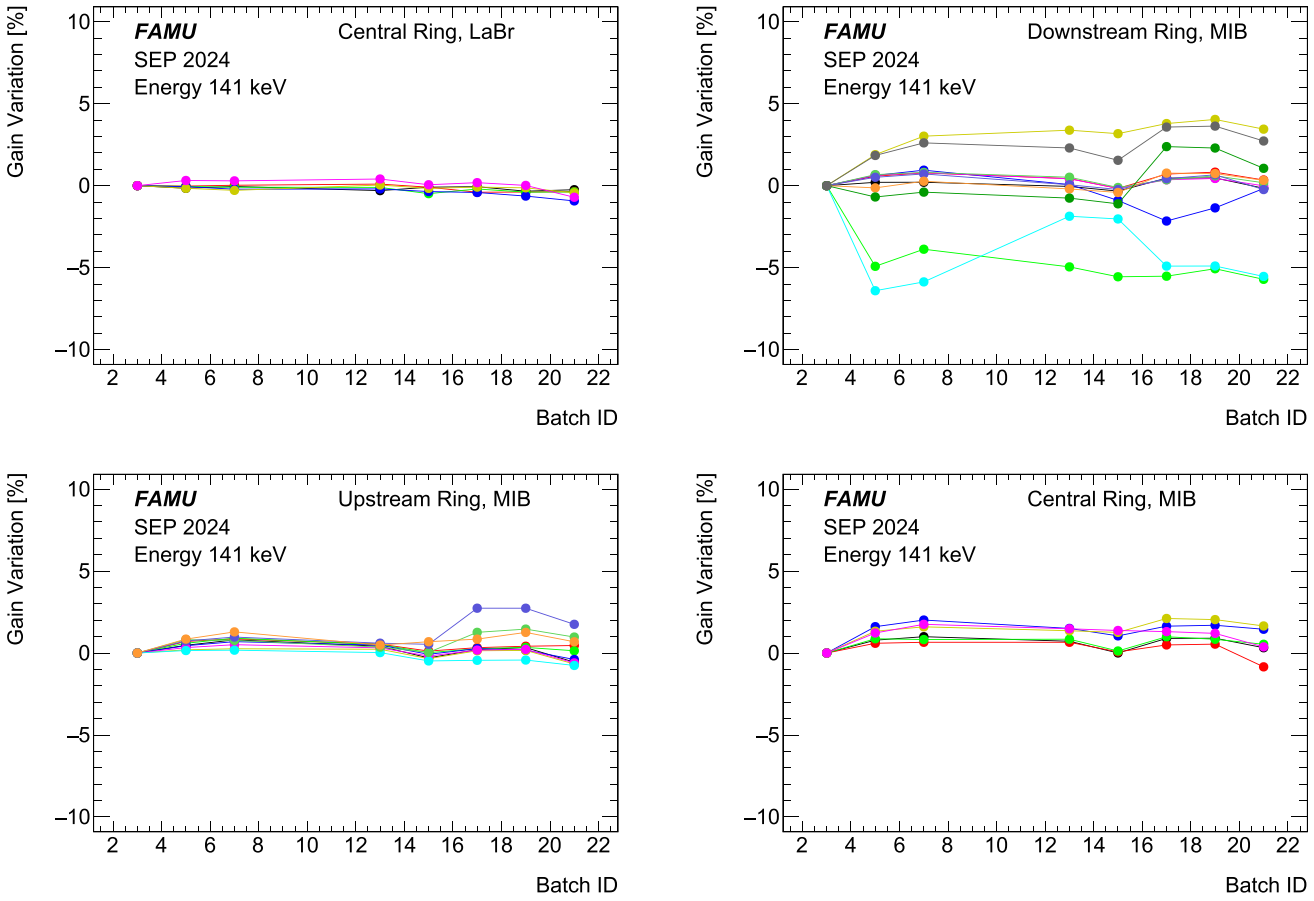

Fig. 15 Gain variation as a function of the time of $LaBr_3$:Ce detectors with PMT (*LaBr*, top-left) and SiPM (*MIB*, other panels) readout. The time on the x-axis is expressed in terms of the batch identification number (*Batch N*) used to uniquely identify each data sample within the same data taking period. The gain variation is evaluated as percent difference of the muonic silver peak position (E = 141 keV) measured in each sample with respect to first sample (Batch 3). After offline equalisation along the different batches, the gain variation for SiPM array readout detectors is compatible with zero

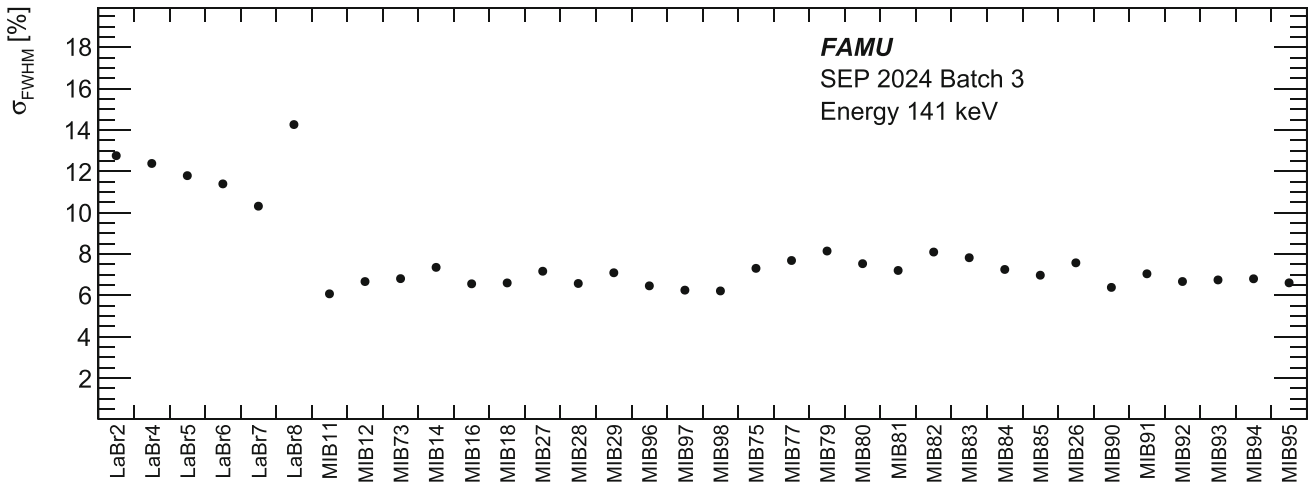

Fig. 16 FWHM energy resolution at 141 keV as a function of the detector name measured in all 34 detectors used in the September 2024 beam time identified by the Batch 3

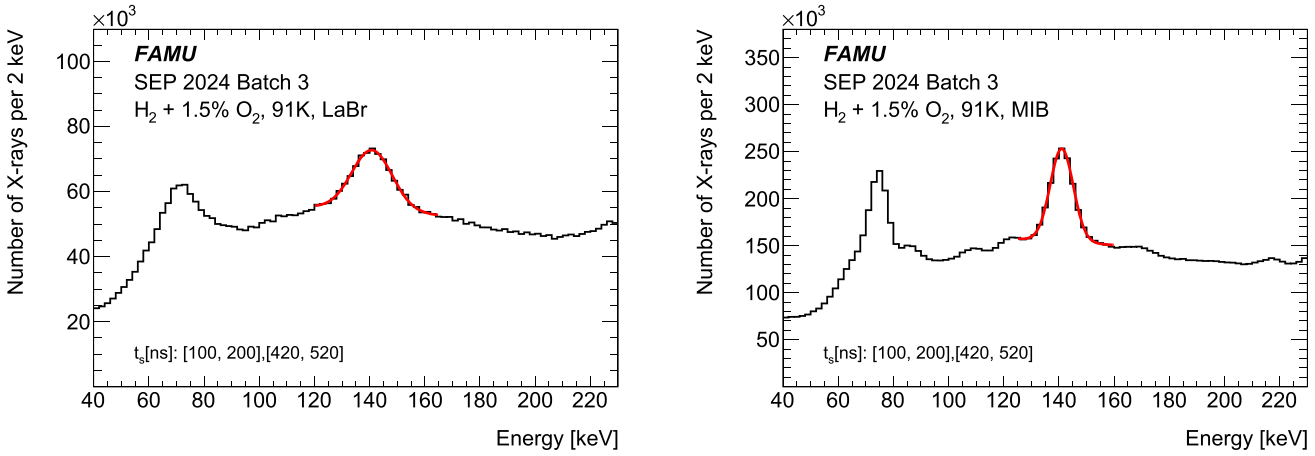

Fig. 17 Calibrated energy spectra (zoom in the region 40÷ 230 keV) obtained by adding up the pulses in all detectors of the same type in the sample with Batch 3. The left plot is obtained using 6 *LaBr* detectors, while the right plot results from the combination of 28 *MIB* detectors. The two peaks at 74 keV and at 141 keV correspond to the prompt X-ray emission following muon beam absorption in Carbon and Silver, respectively. As an example, a Gaussian fit to the data is superimposed in the region around 141 keV assuming a 1-degree polynomial background. The FWHM energy resolution at 141 keV is 12.3% for the combined *LaBr* detectors and 7.0% for the combined *MIB* detectors

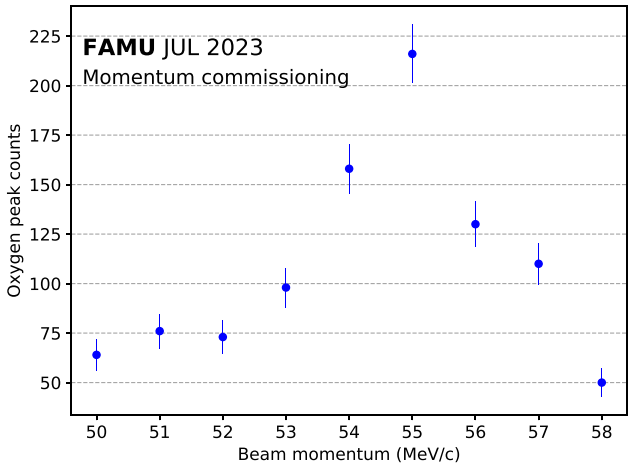

Fig. 18 Variation of the delayed μO X-rays as a function of beam momentum. By selecting $p_\mu = 55$ MeV/c, the number of muons stopped in the gas is maximised

Table 2 Summary of the data acquisition periods with the total statistics of the collected triggers

Period	Setup	No. triggers
Oct 2023	A	1.60×10^7
Dec 2023	A	2.65×10^7
Jul 2024	B	2.12×10^7
Sept 2024	B	2.15×10^7

Setup A and B are described in Sect. 3.4

2024) thanks to the increase of the geometrical acceptance of the X-ray detectors due to the substitution of a number of 0.5″ detectors with 1″ detectors (setup B, see Sect. 3.4).

Figure 22 shows with a black line the spectrum measured in 23 h of data taking in September 2024 with all X-ray detectors and the gas mixture ($H_2 + O_2$). By subtracting the measurement carried out with pure hydrogen in the same period from this one (red filled spectrum in the same plot), it was possible to extract the net oxygen contribution (right panel). Events with energies below the K_α and K_β/K_γ oxygen peaks correspond to X-rays hitting the edges of the crystals, where part of the scintillation light is lost, resulting in a lower recorded energy than expected. The origin of the peak at approximately 110 keV, observed in both the signal and background spectra, is under investigation and may plausibly result from muon- or neutron-induced activation of silver or lead within the target.

The following step towards the final *1S-hfs* measurement would then be the evaluation of the total delayed μO emission rate, separating the collected events in laser and no-laser sub-datasets. In fact, any net signal would have to show up as illustrated in Fig. 2 (left). The actual separation of data in laser and no-laser sub-datasets is currently under investigation, aiming at a blinded analysis protocol. In this way, cognitive biases in the finding of hints of signal in given areas of the spectrum should be avoided. However, before this unblinding can be done, it is still important to set up a testing protocol for systematics to make sure that they are not conditioning the collected data. A first result on the *1S-hfs* of the muonic hydrogen from the FAMU Collaboration will then follow.

5 Conclusions

The FAMU experiment, designed for a high-precision measurement of the hyperfine splitting in muonic hydrogen, reached its final stage in the summer of 2023 after years of

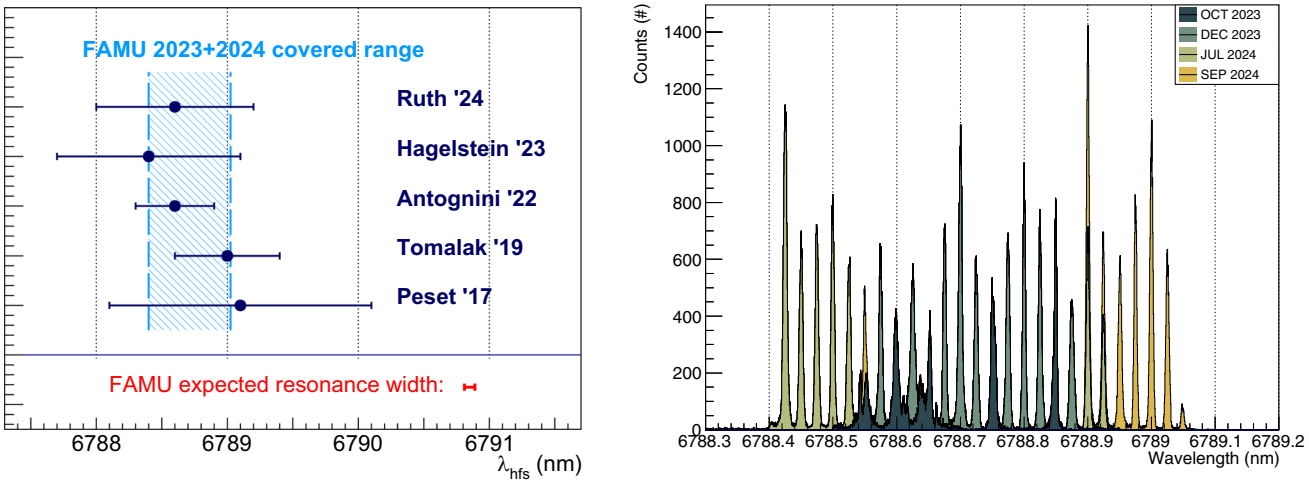

Fig. 19 Left: comparison among the latest theoretical predictions for the *1S-hfs* and the spectral range covered in the 2023 and 2024 beam times. Right: histogram of the 29 wavelengths measured in 2023 and 2024 by the FAMU experiment

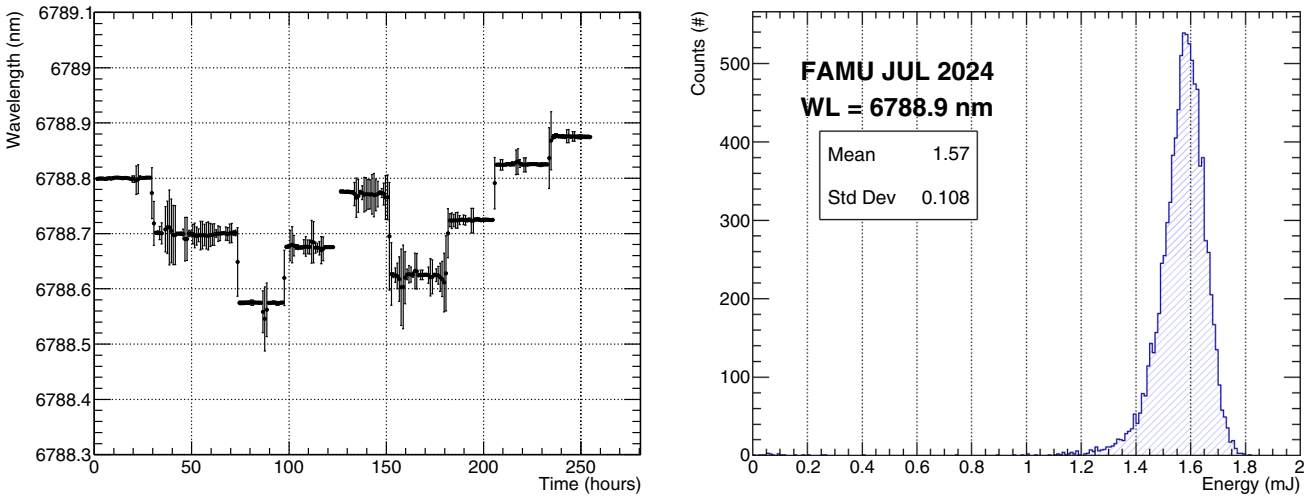

Fig. 20 Left: plot of measured wavelengths as a function of time during the December 2023 run, evidencing the excellent stability due to the automatic wavelength keeping software. Right: example of energy distribution during a batch of data acquisition with fixed wavelength

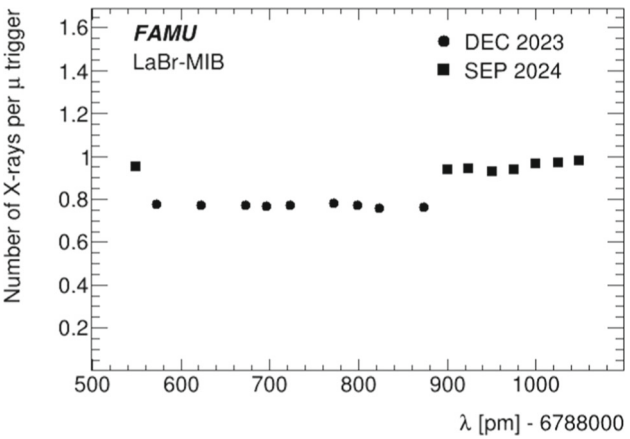

Fig. 21 Number of X-rays per muon trigger collected in the Oxygen signal region by all $LaBr_3$:Ce detectors (*LaBr-MIB*), as a function of the wavelength in two different data taking periods

technological and methodological development. For the first time, the final layout was exposed to the RIKEN-RAL muon beam in its fully operational configuration. All FAMU subdetectors were thoroughly characterised, and their performance was validated before the start of physics runs, which began in the fall of 2023. A key component of the experiment is the FAMU MIR laser, whose unprecedented characteristics and energy delivery enable the excitation of a large number of muonic hydrogen atoms, significantly increasing the statistics of collected X-rays.

The first physics runs confirmed the flawless operation of the experimental setup, allowing for a precise wavelength scan within the range predicted by the latest theoretical studies for the hyperfine resonance of muonic hydrogen. Following data analysis, the refinement of analytical methodologies, and the evaluation of systematic uncertainties, the FAMU

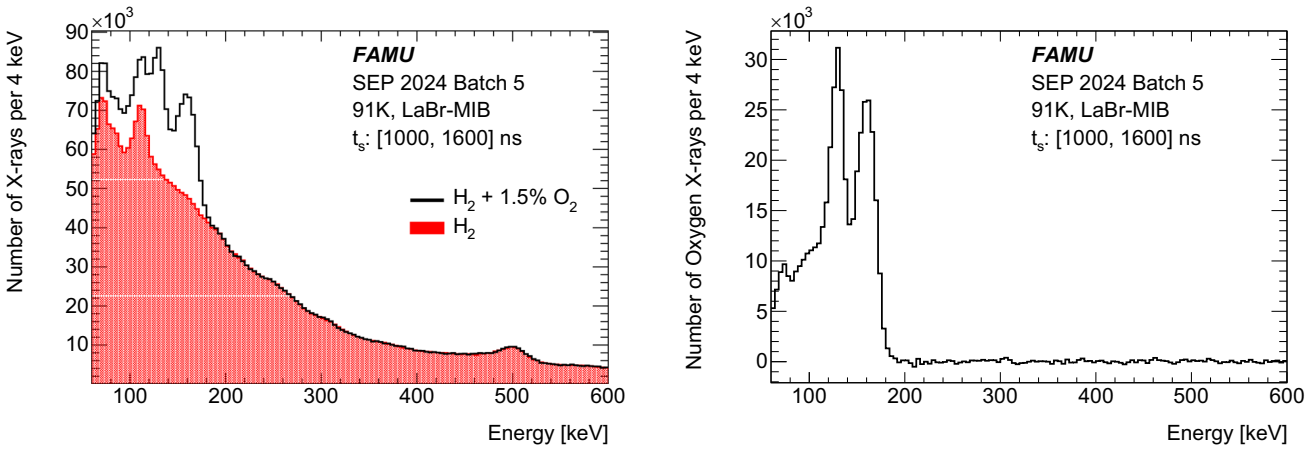

Fig. 22 Subtraction of the normalised H_2 delayed background, measured in September 2024, from the delayed spectrum in Batch 5, for all $LaBr_3$:Ce detectors (*LaBr-MIB*). The plot on the left shows the two spectra, the plot on the right the net subtraction which is the net oxygen contribution

Collaboration will be able to present its first results on the measurement of the hyperfine splitting in muonic hydrogen and, consequently, an assessment of the proton's Zemach radius. FAMU thus has the potential to open a new window into the proton's structure, probing it with unprecedented precision.

Acknowledgements Authors would like to thank RIKEN-RAL and ISIS-STFC for the beam time and technical support during experiments (beamtime reference number RB2000022). We are grateful for the constant support of the INFN CSN3 financing board. We thank Elettra for support on the laser work, and in particular, the SPIE-ICTP Anchor Research Program funded generously by the International Society for Optics and Photonics (SPIE). Authors are grateful to the Italian Ministry for University and Research (MUR) for supporting the FAMU collaboration through the PRIN 2022 Project No. 2022KMNSR9, entitled *"MEtrology and Nonlinear optics for Precision muonic HYdrogen physicS"* (MENPHYS). The research activity presented in this paper has been carried out with the partial support from the Bulgarian Science Fund Grant KP-06-N58/5. The collaborative support of Criotec Impianti srl. in designing, manufacturing, and operating the cryogenic targets that allowed the development of the final layout must be emphasised. We would like to also thank Andrea Abba and Francesco Capogno of Nuclear Instruments for their help in the electronics of the $LaBr_3$:Ce detectors with SiPM readout. The skilful help of the INFN Milano Bicocca and INFN Trieste mechanics workshops for the experimental setup is gratefully acknowledged, as well as the precious contribution by INFN Pavia electronic service, in particular from Marco C. Prata. We extend our gratitude to Lorenzo Panico of the INFN Naples mechanical workshop for the realisation of the two identical multi-pass cavities.

Funding Open access funding provided by Università degli Studi di Pavia within the CRUI-CARE Agreement.

Data Availability Statement This manuscript has no associated data. [Author's comment: Data sharing is not applicable to this article as no datasets were generated or analysed during the current study.]

Code Availability Statement This manuscript has no associated code/software [Author's comment: Code/Software sharing is not applicable to this article as no code/software was generated or analysed during the current study.]

References

1. A. Antognini et al., Proton structure from the measurement of 2S–2P transition frequencies of muonic hydrogen. Science **339**, 417–420 (2013)
2. R. Pohl et al., Muonic hydrogen and the proton radius puzzle. Annu. Rev. Nucl. Part. Sci. **63**, 175–204 (2013)
3. D. Bakalov et al., Experimental method to measure the hyperfine splitting of muomic hydrogen (μ-p)1S. Phys. Lett. A **172**, 277–280 (1993)
4. A. Dupays et al., Proton Zemach radius from measurements of the hyperfine splitting of hydrogen and muonic hydrogen. Phys. Rev. A **68**, 052503 (2003)
5. A. Antognini et al., The proton structure in and out of muonic hydrogen. Ann. Rev. Nucl. Part. Sci. **72**, 389–418 (2022)
6. A.C. Zemach, Proton structure and the hyperfine shift in hydrogen. Phys. Rev. **104**, 1771 (1956)
7. V. Pascalutsa et al., Theoretical discrepancies in the nucleon spin structure and the hyperfine splitting of muonic hydrogen, in *Proceedings of the 10th International Workshop on Chiral Dynamics - CD2021*, vol. 102 (2024)
8. C.E. Carlson et al., Proton-structure corrections to hyperfine splitting in muonic hydrogen. Phys. Rev. A **83**, 042509 (2011)
9. S.G. Karshenboim, Precision physics of simple atoms: QED tests, nuclear structure and fundamental constants. Phys. Rep. **422**, 1 (2005)

10. A. Adamczak et al., On the use of a H_2-O_2 gas target in muonic hydrogen atom hyperfine splitting experiments. Hyperfine Interact. **136**, 1 (2001)
11. A. Adamczak et al., Hyperfine spectroscopy of muonic hydrogen and the PSI Lamb shift experiment. Nucl. Instrum. Methods B **281**, 72–76 (2012)
12. C. Pizzolotto, (FAMU Collaboration) et al., The FAMU experiment: muonic hydrogen high precision spectroscopy studies. Eur. Phys. J. A **56**, 185 (2020)
13. S. Kanda et al., Measurement of the proton Zemach radius from the hyperfine splitting in muonic hydrogen atom. J. Phys: Conf. Ser. **1138**, 012009 (2018)
14. P. Amaro et al., Laser excitation of the 1s-hyperfine transition in muonic hydrogen. Sci. Post Phys. **13**, 020 (2022)
15. A. Adamczak et al., The FAMU experiment at RIKEN-RAL to study the muon transfer rate from hydrogen to other gases. JINST **13**, P12033 (2018)
16. M. Stoilov et al., Experimental determination of the energy dependence of the rate of the muon transfer reaction from muonic hydrogen to oxygen for collision energies up to 0.1 eV. Phys. Rev. A **107**, 032823 (2023)
17. A. Antognini, International Conference on Laser Spectroscopy, ICOLS 2015, Singapore. (2015). arXiv:1512.01765
18. M. Sato et al., Proceedings of the 20th Particles and Nuclei International Conference. Hamburg (2014). https://doi.org/10.3204/DESY-PROC-2014-04/67
19. A. Adamczak, (FAMU Collaboration), et al., Steps towards the hyperfine splitting measurement of the muonic hydrogen ground state: pulsed muon beam and detection system characterization. JINST **11**, P05007 (2016)
20. A. Vacchi, (FAMU Collaboration), et al. RIKEN Accel. Prog. Rep. **49** (2016)
21. A. Vacchi, (FAMU Collaboration), et al., RIKEN Accel. Prog. Rep. **50** (2017)
22. E. Mocchiutti (FAMU Collaboration), et al., FAMU: study of the energy dependent transfer rate $\Lambda_{\mu p \to \mu O}$. J. Phys. Conf. Ser. **1138**, 012017 (2018)
23. E. Mocchiutti (FAMU Collaboration), et al., First measurement of the temperature dependence of muon transfer rate from muonic hydrogen atoms to oxygen. Phys. Lett. A **384**, 126667 (2020)
24. C. Pizzolotto (FAMU Collaboration), et al., Measurement of the muon transfer rate from muonic hydrogen to oxygen in the range 70–336 K. Phys. Lett. A **403**, 127401 (2021)
25. A.D. Hillier et al., Muons at ISIS. Philos. Trans. R. Soc. A **377**(2137), 20180064 (2019)
26. J.W.G. Thomason, The ISIS spallation neutron and muon source-The first thirty-three years. Nucl. Instrum. Methods **A917**, 61 (2019)
27. R. Carbone et al., The fiber-SiPMT beam monitor of the R484 experiment at the RIKEN-RAL muon facility. JINST **12**, C03007 (2015)
28. M. Bonesini et al., The construction of the Fiber-SiPM beam monitor system of the R484 and R582 experiments at the RIKEN-RAL muon facility. JINST **12**, C03035 (2017)
29. M. Bonesini et al., The upgraded beam monitor system of the FAMU experiment at RIKEN-RAL. Nucl. Instrum. Methods **A936**, 592 (2019)
30. R. Rossini (FAMU Collaboration), et al., The muon beam monitor for the FAMU experiment: design, simulation, test, and operation. Front. Detect. Sci. Technol. **2**, 1438902 (2024)
31. M. Baruzzo et al., A mid-IR laser source for muonic hydrogen spectroscopy: the FAMU laser system. Opt. Laser Technol. **179**, 111375 (2024)
32. L.I. Stoychev et al., DFG-based mid-IR laser system for muounic-hydrogen spectroscopy. Laser Sources and Appl. II Proc. **9135**, 91350J (2014)
33. L.I. Stoychev et al., *Increasing the Output Energy of MID-IR Laser System for Muounic-hydrogen Spectroscopy*, 2015 Fotonica AEIT Ital. Conf. Photonics Technol. Turin Italy May 6–8 (2015)
34. L.I. Stoychev et al., Pulse amplification in a Cr4+:forsterite single longitudinal mode (SLM) multi-pass amplifier. Laser Phys. **29**, 065801 (2019)
35. L.I. Stoychev et al., DFG-based mid-IR tunable source with 0.5 mJ energy and a 30 pm linewidth. Opt. Lett. **45**, 5526 (2020)
36. G. Baldazzi et al., The $LaBr_3$(Ce) based detection system for the FAMU experiment. JINST **12**, C03067 (2017)
37. M. Bonesini et al., Large area $LaBr_3$: Ce crystals read by SiPM arrays with improved timing and temperature gain drift control. Nucl. Instrum Methods A **1046**, 167677 (2022)
38. M. Bonesini et al., *One inch LaBr3:Ce detectors, with temperature control and improved time resolution for low energy X-rays spectroscopy*. PoS (EPS-HEP2023), 547 (2023)
39. M. Bonesini et al., Ce:LaBr 3 crystals with SiPM array readout and temperature control for the FAMU experiment at RAL. JINST **15**, C05065 (2020)
40. M. Bonesini et al., *Detection of low-energy X-rays with 1/2 and 1 inch LaBr3:Ce crystals read by SIPM arrays*, PoS (EPS-HEP2021), 770 (2021)
41. R. Rossini et al., Status of the detector setup for the FAMU experiment at RIKEN-RAL for a precision measurement of the Zemach radius of the proton in muonic hydrogen. JINST **19**, C02034 (2024)
42. R. Rossini (FAMU Collaboration), et al., The 2024 LaBr(Ce) detector setup for the FAMU experiment. Nucl. Instrum. Methods **A1069**, 169953 (2024)
43. M. Bonesini et al., Improving the time resolution of large area LaBr 3: Ce detectors with SiPM array readout. Condens. Matter **8**, 99 (2023)
44. N. Otte et al., Characterization of three high efficiency and blue sensitive silicon photomultipliers. Nucl. Instr. Methods **A846**, 106 (2017)
45. M. Bonesini et al., Online control of the gain drift with temperature of SiPM arrays used for the readout of LaBr 3: Ce crystals. JINST **17**, C10004 (2022)
46. M. Bonesini, The fast X-ray detector system of the FAMU experiment at RAL. Nucl. Instrum. Methods A **1080**, 170780 (2025)
47. M. Soldani et al., High performance DAQ for muon spectroscopy experiments. Nucl. Instrum. Methods A **936**, 327 (2019)
48. F. Hagelstein et al., Chiral perturbation theory of the hyperfine splitting in (muonic) hydrogen. Eur. Phys. J. C **83**, 762 (2023)
49. D. Ruth et al., New spin structure constraints on hyperfine splitting and proton Zemach radius. Phys. Lett. B **859**, 139116 (2024)
50. O. Tomalak, Two-photon exchange correction to the lamb shift and hyperfine splitting of S levels. Eur. Phys. J. A **55**, 64 (2019)
51. C. Peset et al., Model-independent determination of the two-photon exchange contribution to hyperfine splitting in muonic hydrogen. J. High Energy Phys. **04**, 060 (2017)
52. M. Baruzzo et al., *Long-Term Performance of a Mid-IR Laser System for Muonic Hydrogen Spectroscopy: Insights from the FAMU Experiment*, pre-print: https://doi.org/10.2139/ssrn.5464154